FORCE AND POSITION SCALING LIMITS FOR STABILITY IN FORCE REFLECTING TELEOPERATION

Pete Shull*
Stanford Telerobotics Laboratory
Department of Mechanical Engineering
Stanford University
Stanford, California 94305
Email: pshull@stanford.edu

Günter Niemeyer
Stanford Telerobotics Laboratory
Department of Mechanical Engineering
Stanford University
Stanford, California 94305

ABSTRACT

Many telerobotic systems require the use of a slave robot with large inertial and frictional properties. Using a force sensor on the end effector can hide the slave's inertia and friction from the user providing a more accurate sense of the environment, but introduces dangers of system instability.

Both the position and force scale directly affect the system loop gain and hence stability. This opens up the possibility of trading off between them based on the environment and task. In this paper we derive explicit limits for their product. In particular we consider varying environment stiffnesses, as well as distinguishing impact and contact phases. The theoretical limits closely align with experimental results using a large slave telerobotic system interacting with very soft to nearly rigid environments.

INTRODUCTION

Telerobotics seeks to combine the strength, precision, and robustness of a robot with the intelligence and real-time decision making skills of a human. This cooperation enables robots to perform more complex tasks in unstructured environments. In particular, since its first appearance, telerobotics has been proposed and used for a variety of tasks including robotic space repair, [1, 2], deep-sea and nuclear environments [3], and medical robotic surgery [4, 5]. Some of these tasks require the use of a strong and stiff slave robot. These robots are excellent for completing tasks requiring strength and precision surpassing that of humans, but they also possess relatively high inertial and frictional properties. If traditional passivity based controllers are used [6, 7], the slave robot's inertia and friction will be transmitted to the human operator making telemanipulation cumbersome and awkward. The slave's high friction can further cause the robot to become non-backdrivable severely limiting the user's sense of haptic feeling of the environment.

Force sensors can be used on the slave's end-effector to deal with the negative effects of high friction and high inertia. By feeding back environment forces directly, the slave's inertia and friction are hidden from the user by providing a direct sense of touch of the environment. This force reflecting system can provide the user with a more accurate sense of transparency [8] but can also tend toward instability. Local force feedback has been proposed as a method of hiding the slave's large inertial and frictional properties and increasing the slave's environment sensitivity while simultaneously maintaining overall system stability [9,10]. It is also possible to use the measured and estimated environment force for stable force loop control on environments of varying stiffnesses [11].

All force reflecting teleoperation systems utilizing an end effector force sensor are prone to closed-loop instabilities and thus must adhere to certain overall loop gain limitations. The maximum closed-loop gain is dependent on a variety of system properties including master/slave inertia and damping, overall loop time delay, force/position scaling, and environment stiffness. The environment stiffness acts as a multiplicative gain potentially driving the closed-loop system unstable. For example if the user telerobotically moves the slave robot from contact with a soft environment to contact with a stiff environment, the increase in environment stiffness will likely cause system instability. The product of position and force scaling also acts as a multiplicative gain and can be varied to maintain stability with changing envi-

*Address all correspondence to this author.

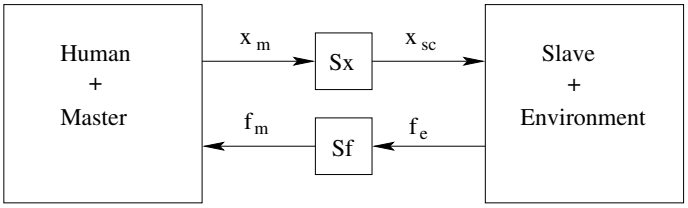

Figure 1. BILATERAL FORCE REFLECTION

ronment stiffness. It may be advantageous to vary position and force scaling unequally. If the slave is contacting a rigid environment, a small position scale may be acceptable, while contact with a soft environment will likely require a larger position scale.

Force-feedback systems are also susceptible to contact instabilities which are triggered by impacts with the environment. During the transition from freespace to environment contact the slave impacts the environment sending back impulsive forces to the user. Because of the slave's high inertia, these impulsive forces can cause discontinuity and repeated bouncing. This can happen particularly when the slave impacts rigid environments. Limiting the magnitude of the impulsive forces appropriately can ensure stability by causing the bouncing to decay quickly or eliminate any bounce.

In order to be able to design control architectures for telerobotic systems with large slave devices which provide the user with useful force feedback, stability must be maintained during all phases of operation. To do this we need to precisely define the scaling limits to avoid impact instabilities during the impact phase and closed-loop instabilities while the slave is in constant contact with the environment.

We endeavor to build off the work of Daniel and McAree [12] by finding explicit equations for the maximum product of force and position scaling during impact and while in constant contact with an environment. We especially consider environments of various stiffnesses and imperfect slave tracking capabilities. We first introduce force reflecting teleoperation, and then derive explicit limitation equations on the product of position and force scales for impact and in-contact phases. Next, we show experimental results and discuss their significance with respect to theoretical predictions. And lastly, we offer concluding remarks.

FORCE REFLECTING TELEOPERATION

Force reflecting bilateral teleoperation can be a useful control architecture for telerobotics when using a large slave robot. The slave's large friction and inertia make using passivity based architectures difficult, because these architectures pass the frictional and inertial forces along to the user. This undesirable effect can be combated by placing a force sensor on the end of the slave robot's end effector and feeding back slave forces directly to the user. In this way the user only feels the environment forces and not the slave's frictional and inertial forces.

Figure 1 shows a general bilateral force reflecting system. In this system the human operator and master device are grouped together on one side of the transmission line and the environment and slave device on the other. The master robot's tip position x_m is scaled by S_x and becomes the slave robot's commanded position x_{sc}. In the feedback path f_e is the measured environment force and f_m the force applied to the master robot found by scaling the environment force by S_f. S_x and S_f act as multiplicative gains on the closed loop system.

We consider three distinct operating phases in teleoperation. In the freespace phase the slave tip moves around freely without contacting the environment. The only forces fed back to the human operator are due to the noise of the force sensor and inertial effects of any tool tip attached to the force sensor. These feedback forces are usually relatively small meaning teleoperation is essentially open loop. The impact phase occurs when the slave first touches the environment from freespace and is dominated by impulsive forces which rapidly decelerate the slave. The in-contact phase occurs while the slave continues to operate in constant contact with the environment. During both the impact phase and in-contact phase the feedback forces displayed to the user are significant,and instabilities will occur for some force and position scaling values. We next seek to derive explicit equations for the maximum product of force and position scaling during the impact and in-contact phases.

IMPACT SCALING LIMITATIONS

During the impact phase as the slave transitions from freespace to contact initially impacting the environment, the environmental impulsive forces are fed back to the user. Large impulsive forces, occurring particularly in cases when the slave has high inertia and the environment is very stiff, can cause the user's hand to jerk away in the opposite direction of contact. Contact instabilities occur if the master bounces off the surface and in particular if repeated bounces do not decay. This is the case when each bounce introduces energy into the system, i.e. when the magnitude of the user's velocity after impact exceeds the magnitude of the velocity before impact. During impact, the system is practically open-loop, unable to control the force but displaying the scaled impact forces to the master. The duration of impact T_i is determined by either the time required to detect contact and regulate the contact force if the slave itself does not bounce, or the natural frequency of contact if the slave does bounce. In turn, this is determined by the environment stiffness and slave mass, as we derive below.

Figure 2a depicts the master and slave models for the impact phase. As the slave impacts the environment, the environmental impulsive forces tend to dominate the master's dynamics. We examine the worst case when the user is lightly holding on to the master device and the user's stiffness and damping forces are negligible. In this case, if the environmental impact impulse is equal in magnitude and opposite in direction to the initial linear momentum of the master the master's final velocity would

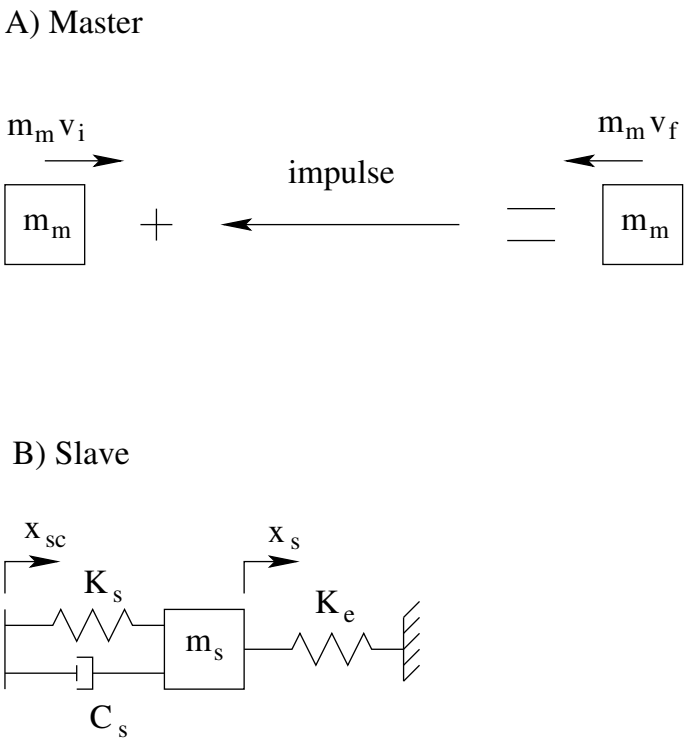

Figure 2. MASTER/SLAVE IMPACT MODEL

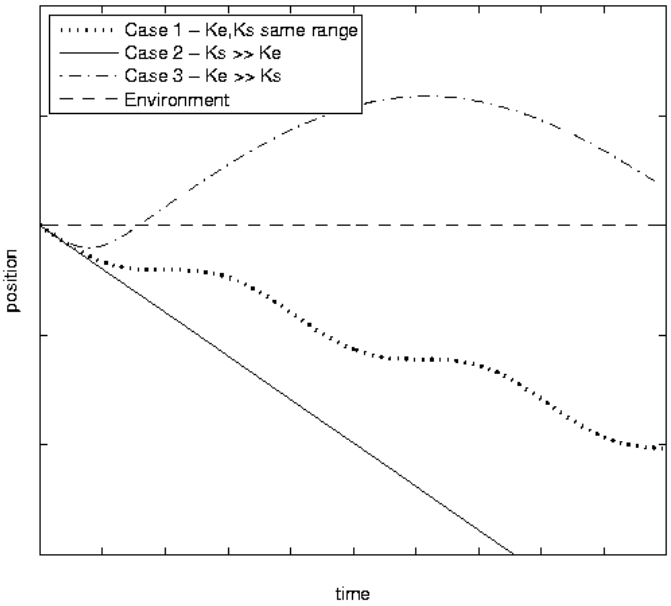

Figure 3. IMPACT FOR DIFFERENT KE/KS

be zero. If the magnitude of the impulse was twice as large as the master's initial linear momentum, the final momentum would be equal in magnitude and opposite in direction. If it was more than twice as large, the master's final linear momentum would be greater than its initial. It's energy will have artificially increased. In this case, the user would encounter contact instabilities repeatedly bouncing off of the environment.

The slave model during impact is shown in figure 2b. The slave's dynamics during impact will largely be affected by relative stiffnesses of the slave's controller K_s and the environment stiffness K_e. If the slave controller stiffness is very large relative to the environment stiffness, the slave will barely be affected during impact but will continue unhindered along its commanded path until the controller reacts. However, if the environment stiffnesses is relatively large, the slave controller will have little power and the slave will quickly be repelled away from contact. If the two stiffnesses are in the same range, they will compete and the response will be a combination of the two. Figure 3 shows the general slave response during impact for the three cases described. In case 1 K_e and K_s are in the same range, in case 2, $K_s \gg K_e$, and in case 3, $K_e \gg K_s$.

To derive maximum limits on the force and position scaling during impact, we should first notice that the absolute value of the master's final velocity just after impact must be less than the master's initial velocity just before impact in order for energy to be removed and bounces to decay to avoid contact instabilities.

$$|\dot{x}_{mf}| < |\dot{x}_{mi}| \tag{1}$$

Also, we can write the master's impulse-momentum equation by inspecting figure 2a

$$m_m \dot{x}_{mi} - \int_0^{T_i} f_m(t)dt = -m_m \dot{x}_{mf} \tag{2}$$

where the impulsive force applied to the master, $f_m(t)$ is integrated from the instant of impact at time 0 until the end of impact at time T_i. Rearranging this equation, we get

$$\int_0^{T_i} f_m(t)dt = m_m(\dot{x}_{mi} + \dot{x}_{mf}) \tag{3}$$

The length of impact T_i is the shorter time of either the system time delay or the time constant of the environment and slave (i.e. the time required for the slave to bounce off a stiff environment). Knowing from (1) that the maximum value of $\dot{x}_{mf}$ is $\dot{x}_{mi}$ we arrive at the inequality

$$\int_0^{T_i} f_m(t)dt < 2m_m \dot{x}_{mi} \tag{4}$$

If this inequality is not satisfied then the impact bounces will never decay. We next write the slave's equations of motion from figure 2b taking into account only the dominating effects of the slave controller stiffness and the environment stiffness.

$$m_s\ddot{x}_s + K_e x_s + K_s(x_s - x_{sc}) = 0 \tag{5}$$

We assume that during the short time of impact the slave's commanded position is related to the master's initial velocity and the position scale factor

$$x_{sc} = S_x\dot{x}_{mi} \cdot t \tag{6}$$

Similarly, the slave's initial velocity and master's initial velocity during impact are related by the position scale factor

$$\dot{x}_{si} = S_x\dot{x}_{mi} \tag{7}$$

Substituting (6) into (5) and rearranging we get a differential equation for the slave's motion during impact

$$\ddot{x}_s + \frac{K_e + K_s}{m_s} \cdot x_s - \frac{K_s S_x \dot{x}_{mi}}{m_s} \cdot t = 0 \tag{8}$$

Using Laplace and inverse Laplace transforms and noting (7) we arrive at a time dependent equation describing the slave's position during impact

$$x_s(t) = S_x\dot{x}_{mi}\left[\frac{K_e\sqrt{m_s}}{(K_e+K_s)^{3/2}} \cdot \sin\left(\sqrt{\frac{K_e+K_s}{m_s}} \cdot t\right) + \frac{K_s}{K_e+K_s} \cdot t\right] \tag{9}$$

The environment force is related to the slave position by the environment stiffness

$$f_e(t) = K_e x_s(t) \tag{10}$$

and the force applied to the master is related to the environment force by the force scaling factor (see figure 1)

$$f_m(t) = S_f f_e(t) \tag{11}$$

Combining (9), (10), and (11), we get the force applied to the master during impact as a function of time.

Case	Condition	Max S_xS_f
1	none	$\frac{m_m}{K_e\left[\frac{K_e m_s}{2(K_e+K_s)^2}\cdot\left(1-\cos\left(\sqrt{\frac{K_e+K_s}{m_s}}\cdot T_i\right)\right)+\frac{K_s}{4(K_e+K_s)}\cdot T_i^2\right]}$
2	$K_s \gg K_e$	$\frac{m_m}{\frac{1}{4}K_e T_d^2}$
3	$K_e \gg K_s$	$\frac{m_m}{m_s}$

Table 1. IMPACT LIMITATIONS TABLE

$$f_m(t) = S_x S_f K_e \dot{x}_{mi}\left[\frac{K_e\sqrt{m_s}}{(K_e+K_s)^{3/2}} \cdot \sin\left(\sqrt{\frac{K_e+K_s}{m_s}} \cdot t\right) + \frac{K_s}{K_e+K_s} \cdot t\right] \tag{12}$$

Substituting (12) into (4) and solving for S_xS_f we obtain an inequality bounding the maximum product of position and force scaling during impact.

$$S_xS_f < \frac{m_m}{K_e\left[\frac{K_e m_s}{2(K_e+K_s)^2}\cdot\left(1-\cos\left(\sqrt{\frac{K_e+K_s}{m_s}}\cdot T_i\right)\right)+\frac{K_s}{4(K_e+K_s)}\cdot T_i^2\right]} \tag{13}$$

This general equation (13) is valid for any K_s and K_e. Let's now look at the specific cases from figure 3. In case 2 the slave controller's stiffness is much greater than the environment stiffness $K_s \gg K_e$. From (13) we multiply the first term in the denominator by $\frac{K_s^2}{K_s^2}$ and the second term by $\frac{K_s}{K_s}$ to get

$$S_xS_f < \frac{m_m}{K_e\left[\frac{\frac{K_e}{K_s^2}m_s}{2(\frac{K_e^2}{K_s^2}+\frac{K_eK_s}{K_s^2}+\frac{K_s^2}{K_s^2})}\cdot\left(1-\cos\left(\sqrt{\frac{K_e+K_s}{m_s}}\cdot T_i\right)\right)+\frac{\frac{K_s}{K_s}}{4(\frac{K_e}{K_s}+\frac{K_s}{K_s})}\cdot T_i^2\right]} \tag{14}$$

As $\frac{K_e}{K_s} \to 0$, the first term in the denominator approaches zero and the second term approaches $\frac{1}{4}T_i^2$. In this case T_i will be the length of time it takes the closed loop system to respond to controlling commands, which is the closed loop time delay, T_d. After substituting T_d in for T_i, we arrive at the final inequality when $K_s \gg K_e$

$$S_xS_f < \frac{m_m}{\frac{1}{4}K_e T_d^2} \tag{15}$$

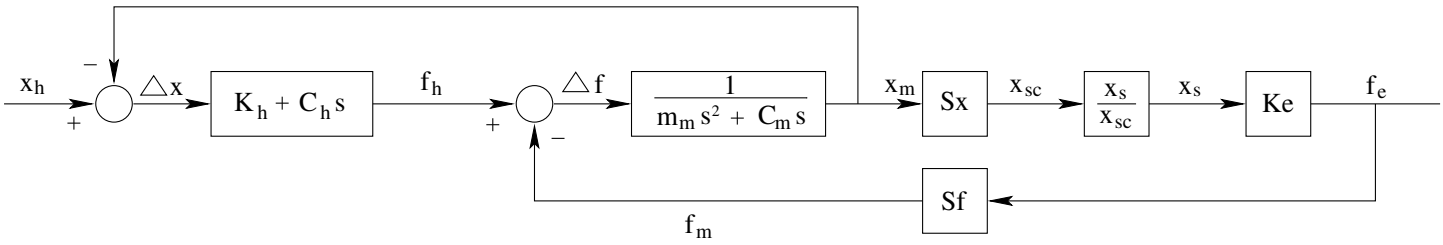

Figure 4. IN-CONTACT BLOCK DIAGRAM

We now examine case 3 from figure 3 when $K_e \gg K_s$. We first assume that the contact time will be very short because of the high environment stiffness and note that T_i will no longer be the entire system loop time delay but will instead be $\frac{1}{2}$ of the period determined by the natural frequency of the environment and controller stiffness and the slave mass

$$T_i = \frac{\pi}{\sqrt{\frac{K_e+K_s}{m_s}}} \tag{16}$$

After substituting (16) into (13) and multiplying the first and second terms in the denominator by $\frac{K_e^2}{K_e^2}$, we note that as $\frac{K_s}{K_e} \to 0$ the first term in the denominator approaches $\frac{m_s}{K_e}$ and the second term approaches zero. Simplifying this result, we find that the final inequality when $K_e \gg K_s$ is

$$S_x S_f < \frac{m_m}{m_s} \tag{17}$$

This result shows that in the case when the environment stiffness is much greater than the controller stiffnesses the maximum scaling is bounded by the mass ratio. This aligns with the work of Daniel and McAree [12]. Table 1 shows the scaling limitation results for each case during impact.

IN-CONTACT SCALING LIMITATIONS

The in-contact phase begins after the slave has impacted the environment and the impulsive forces have decayed. It lasts until the slave breaks away from the environment. The environmental forces will generally be relatively smaller than the impulsive impact forces, and thus we should take into account human operator forces and damping forces. Figure 4 shows the closed loop block diagram during the contact phase. We notice that environment forces as well as forces from the master device damping, human operator damping, and human operator stiffness all contribute to the movement of the of the master device. We also note the general transfer function relating the slave's commanded position to the slave's actual position is $\frac{x_s}{x_{sc}}$. If the effective slave controller stiffness is much larger than the environment stiffness, then $\frac{x_s}{x_{sc}}$ will be the same in freespace and in-contact, otherwise this transfer function will depend on the environment stiffness, K_e.

Either through block diagram manipulation or by combining transfer functions algebraically, we can determine $\frac{x_m}{x_h}$, the transfer function relating the desired human position to the master device position

$$\frac{x_m}{x_h} = \frac{\frac{C_h s+K_h}{m_m s^2+(C_h+C_m)s+K_h}}{1+S_x S_f K_e \cdot \frac{x_s}{x_{sc}} \cdot \frac{1}{m_m s^2+(C_h+C_m)s+K_h}} \tag{18}$$

We assume that the transfer function relating the slave's commanded to actual position can be represented as a proportional derivative 2nd order function with a pure time delay.

$$\frac{x_s}{x_{sc}} = \frac{\tilde{C}_s s+\tilde{K}_s}{s^2+\tilde{C}_s s+\tilde{K}_s} \cdot e^{-T_d s} \tag{19}$$

where $\tilde{K}_s$ is the slave controller stiffness over the slave mass $\frac{K_s}{m_s}$, $\tilde{C}_s$ is the slave controller damping over the slave mass $\frac{C_s}{m_s}$, and T_d is the system time delay. The denominator in (18) is the characteristic equation Δ and determines the overall closed loop stability of the system. Substituting (19) into (18) gives the characteristic equation

$$\Delta = 1 + KG(s) \tag{20}$$

where,

$$K = S_x S_f \tag{21}$$

$$G(s) = \frac{K_e(\tilde{C}_s s+\tilde{K}_s)}{(m_m s^2+(C_h+C_m)s+K_h)(s^2+\tilde{C}_s s+\tilde{K}_s)} \cdot e^{-T_d s} \tag{22}$$

We want the system stability to be independent of how tightly the user is holding on to the master device. Since a tighter grip will increase stability, we look at the worst case when the user is not holding on where C_h and K_h are zero. Setting $C_h = K_h = 0$ and rearranging (22) into bode form yields

$$G(s) = \frac{K_e}{C_m} \cdot \frac{\frac{\tilde{C}_s}{\tilde{K}_s}s + 1}{s(\frac{m_m}{C_m}s+1)(\frac{1}{\tilde{K}_s}s^2 + \frac{\tilde{C}_s}{\tilde{K}_s}s + 1)} \cdot e^{-T_d s} \qquad (23)$$

We can compare (23) to a general form bode equation to determine the relevant cutoff frequencies and damping ratios

$$G(s) = \frac{K_e}{C_m} \cdot \frac{\frac{1}{\omega_1}s + 1}{s(\frac{1}{\omega_2}s+1)(\frac{1}{\omega_3^2}s^2 + \frac{2\zeta_3}{\omega_3}s + 1)} \cdot e^{-T_d s} \qquad (24)$$

One way to determine system stability is to perform a Nyquist analysis on the characteristic equation (20). The gain $K = S_x S_f$ can then be adjusted accordingly to achieve stability. Here we seek to obtain an explicit equation for the allowable range of $S_x S_f$ for system stability based on inherent system properties. A conservative approach is to confine the magnitude of $KG(s)$ to be less than one at the frequency of the zero in $G(s)$.

$$\left| KG(s) \right|_{s=j\omega_1 = j\frac{\tilde{K}_s}{\tilde{C}_s}} < 1 \qquad (25)$$

ω_1 is generally slower than the other cutoff frequencies and thus the negative contribution to phase margin from the system time delay, slave controller's poles, and master mass/damping before ω_1 are fairly small and not enough to cause instability. The magnitude at ω_1 will be decreasing and will only further decrease at higher frequencies, so restricting the magnitude to less than one at ω_1 should ensure stability for operation at all frequencies. Simplifying and rearranging (25) we arrive at the final inequality bounding the maximum value of the product of S_x and S_f while the slave is in-contact with the environment.

$$S_x S_f < c_1 c_2 \frac{1}{K_e} \qquad (26)$$

where,

$$c_1 = \frac{1}{\sqrt{32}\zeta_3^2}\sqrt{1 + \left(1 - \frac{1}{4\zeta_3^2}\right)^2} \quad \zeta_3 = \frac{\tilde{C}_s}{2\sqrt{\tilde{K}_s}} \qquad (27)$$

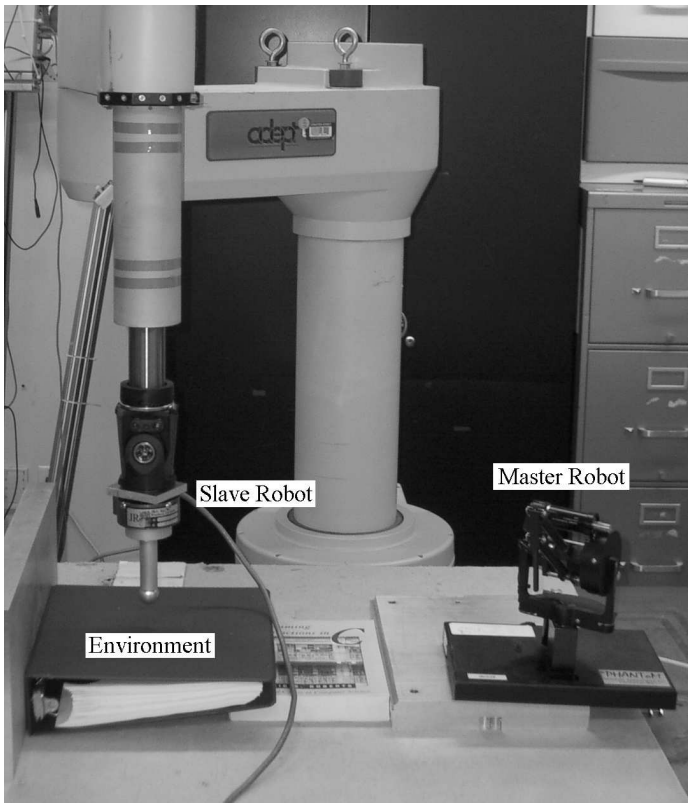

Figure 5. EXPERIMENTAL SETUP

$$c_2 = \sqrt{(\tilde{K}_s m_m)^2 + (\tilde{C}_s C_m)^2} \qquad (28)$$

EXPERIMENTAL VALIDATION

To validate the theoretical limitations on $S_x S_f$ derived in the previous two sections, we performed tests during impact and in-contact with a teleoperation system. We use an experimental setup, as presented in figure 5. The master robot is a Phantom haptic device capable of updating forces and measuring positions on a master computer in realtime at a rate of 1 kHz. The Phantom has low inertial and frictional properties and is thus suited well as a master teleoperator device [13]. The slave is an AdeptOne 5-axis Scara industrial robot [14, 15]). It has high frictional and inertial properties. The Adept is able to receive position commands at a rate of $62.5hz$ from a slave computer which also reads the contact force sensor. Communications between the master and slave are achieved through a network using the TCP protocol. The overall system time delay was $64ms$

We first seek to determine the experimental limits on $S_x S_f$ during the impact phase. The effective controller stiffness of the Adept was much larger than the environmental stiffnesses tested $K_s \gg K_e$ and thus its limitations were of case 2 (15). For testing, a user held the master device and pulled it downward until

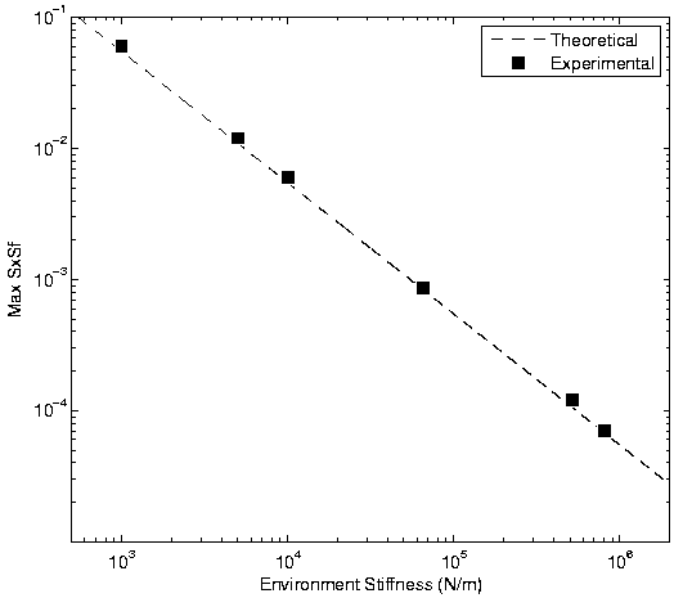

Figure 6. MAX SxSf FOR IMPACT STABILITY

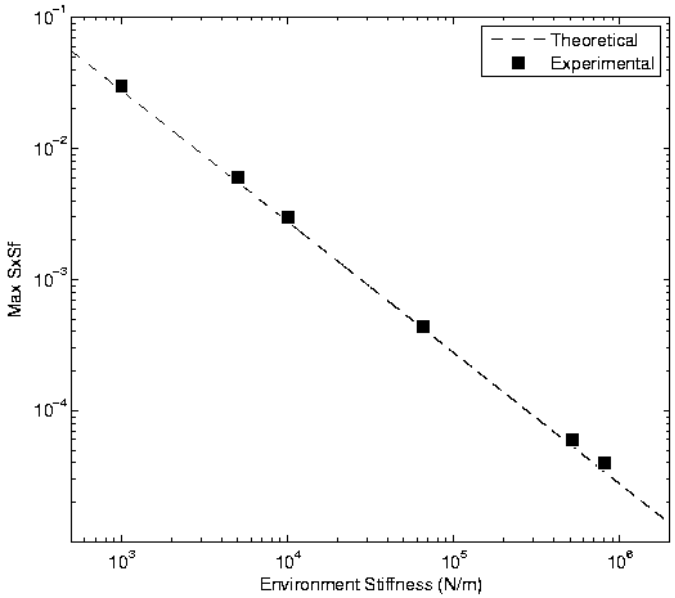

Figure 7. MAX SxSf FOR IN-CONTACT STABILITY

the slave impacted the environment. Environments of varying stiffness ranging from $1000\frac{N}{m}$ (soft foam) to $810,000\frac{N}{m}$ (solid aluminum block) were used. Data was collected and then analyzed to determine the initial and final velocity during the impact phase. The maximum S_xS_f occurred when the value of the initial and final velocities had the same magnitude but opposite direction, i.e. the initial and final master energies were the same.

To determine the max S_xS_f during the in-contact phase, the human operator first released the master device so that $C_h = K_h = 0$. S_x and S_f were set to very low values and then a small downward offset force was applied to the master causing it to move downward until the slave made contact with the environment. After the slave and master were in-contact stably, a small step offset force was added to the preexisting offset force. If the system was able to achieve stability after the step input, the trial was repeated using a higher S_xS_f value. If the offset step input caused the system to go unstable S_xS_f was scaled back. This process was repeated until an offset step input caused the system to barely maintain stability and the corresponding S_xS_f value was deemed the maximum. This was repeated for environments varying in stiffness from $1000\frac{N}{m}$ to $810,000\frac{N}{m}$.

RESULTS/DISCUSSION

Figure 6 shows the theoretical and experimental results for the impact phase. The theoretical dashed line for impact stability was obtained by using the system parameters $m_m = 0.056kg$ and $T_d = 0.064s$ in (15) while varying K_e. Experimental data points (black squares) were obtained at environment stiffnesses of $K_e = 1000\frac{N}{m}$, $5000\frac{N}{m}$, $10,000\frac{N}{m}$, $65,000\frac{N}{m}$, $520,000\frac{N}{m}$, and $810,000\frac{N}{m}$. The experimental data points are all only slightly higher than the theoretical maximum which suggests that our theoretical bounding equation (15) is accurate and slightly conservative.

Figure 7 shows the theoretical and experimental results for the in-contact phase. The theoretical line for in-contact stability was obtained by using the system parameters $\tilde{K}_s = 600\frac{N}{kgm}$, $\tilde{C}_s = 50\frac{Ns}{kgm}$, $m_m = 0.056kg$, and $C_m = 2.5\frac{Ns}{m}$ in (26) while varying K_e. Experimental data points were obtained at environment stiffnesses of $K_e = 1000\frac{N}{m}$, $5000\frac{N}{m}$, $10,000\frac{N}{m}$, $65,000\frac{N}{m}$, $520,000\frac{N}{m}$, and $810,000\frac{N}{m}$. Like in the impact phase the experimental data points are all slightly above the theoretical maximum suggesting that the bounding equation (26) is accurate and slightly conservative.

CONCLUSION

In this work we have derived theoretical maximum scaling limits for the product of position and force scaling for the impact and in contact phases. The theoretical limits very closely match experimental results and clearly show the expected inverse relationship to the environment stiffness. Knowledge of the maximum scales allows not only appropriate tuning of bilateral systems, it also opens the possibilities of automatically adjusting scales during operation, trading off position scale in freespace with force scale in contact while maintaining stability in all phases. We hope this work will ultimately bring robots under human control into unstructured environments working with rigid objects, typical of many proposed applications.

ACKNOWLEDGMENT

This work was supported by the National Aeronautics and Space Administration via the Institute for Space Robotics.

REFERENCES

[1] Parrish, J., 1999. "The ranger telerobotic shuttle experiment: An on-orbit satellite servicer". In 5th International Symposium on Artifical Intelligence, Robotics, and Automation in Space.

[2] Akin, D. L., Roberts, B., Pilotte, K., and Baker, M., 2003. "Robotic augmentation of eva for hubble telescope servicing". In AIAA Space 2003 Conference.

[3] Goertz, R. C., 1952. "Fundamentals of general-purpose remote manipulators". *Nucleonics,* **10**(11), Nov., pp. 36–45.

[4] Tatooles, A. J., Pappas, P. S., Gordon, P. J., and Slaughter, M. S., 2004. "Minimally invasive mitral valve repair using the da vinci robotic system". *The Annals of Thoracic Surgery,* **77**, pp. 1978–1984.

[5] Wykypiel, H., Wetscher, G., Klaus, A., Schmid, T., Gadenstaetter, M., Bodner, J., and Bodner, E., 2003. "Robot-assisted laparoscopic partial posterior fundoplication with the davinci system: Initial experiences and technical aspects". *Langenbeck's Archives of Surgery,* **387**(11), Feb., pp. 411–416.

[6] Niemeyer, G., and Slotine, J.-J. E., 1991. "Stable adaptive teleoperation". *IEEE Journal of Oceanic Engineering,* **16**(1), Jan., pp. 152–162.

[7] Anderson, R. J., and Spong, M. W., 1989. "Bilateral control of teleoperators with time delay". *IEEE Trans. on Automatic Control,* **34**(5), May, pp. 494–501.

[8] Lawrence, D. A., 1993. "Stability and transparency in bilateral teleoperation". *IEEE Transactions on Robotics and Automation,* **9**(5), Oct., pp. 624–637.

[9] Shull, P. B., and Niemeyer, G., 2007. "Experiments in local force feedback for high-inertia high-friction telerobotic systems". In Proc. of IMECE2007.

[10] Hashtrudi-Zaad, K., and Salcudean, S. E., 2002. "Transparency in time delayed systems and the effect of local force feedback for transparent teleoperation". *IEEE Transactions on Robotics and Automation,* **18**(1), Feb., pp. 108–114.

[11] Park, J., and Khatib, O., 2006. "A haptic teleoperation approach based on contact force control". *Int. Journal of Robotics Research,* **25**(5-6), May, pp. 575–591.

[12] Daniel, R. W., and McAree, P. R., 1998. "Fundamental limits of performance for force reflecting teleoperation". *Int. Journal of Robotics Research,* **17**(8), Aug., pp. 811–830.

[13] Cavusoglu, M. C., Feygin, D., and Tendick, F., 2002. "A critical study of the mechanical and electrical properties of the phantom hatpic interface and improvements for high-performance control". *Presence,* **11**(6), pp. 555–568.

[14] Shull, P. B., and Gonzalez, R. V., 2006. "Real-time haptic-teleoperated robotic system for motor control analysis". *Journal of Neuroscience Methods,* **151**(2), Mar., pp. 194–199.

[15] Curran, R., and Mayer, G., 1985. "The architecture of the adeptone direct-drive robot". In Proc. of The American Control Conference, pp. 716–721.